Journal of Cancer Research and Treatment, 2016, Vol. 4, No. 1, 9-16
Available online at http://pubs.sciepub.com/jcrt/4/1/2

DOI:10.12691/jcrt-4-1-2

Single Shot Irradiation and Molecular Effects on a Diffuse Large B Cell Lymphoma Cell Line

Fernando Mendes[1,2,3,4,*], Cátia Domingues[3,5], Susann Schugk[6], Ana Margarida Abrantes[1,3], Ana Cristina Gonçalves[3,5], Tiago Sales[1], Ricardo Teixo[1], Rita Silva[1], Jéssica Estrela[2], Mafalda Laranjo[1,3], João Casalta-Lopes[1,7], Clara Rocha[8,9], Paulo César Simões[7], Ana Bela Sarmento[3,5,10], Maria Filomena Botelho[1,3], Manuel Santos Rosa[11]

[1]Biophysics and Biomathematics Institute, IBILI-Faculty of Medicine, University of Coimbra, Portugal
[2]Polytechnic Institute of Coimbra, ESTESC-Coimbra Health School, Department Biomedical Laboratory Sciences, Coimbra, Portugal
[3]CIMAGO, FMUC-Faculty of Medicine, University of Coimbra, Portugal
[4]CNC.IBILI, Universidade de Coimbra, Portugal
[5]Oncobiology and Hematology Laboratory Applied Molecular Biology and Clinical University of Hematology, Faculty of Medicine of University of Coimbra, Coimbra, Portugal
[6]Biomedical Laboratory Sciences Department, University of Gothenburg
[7]Radiation Oncology Department, Hospital and University Center of Coimbra, Coimbra, Portugal
[8]Polytechnic Institute of Coimbra, ESTESC-Coimbra Health School, Department Complementary Sciences, Coimbra, Coimbra, Portugal
[9]Institute for Systems Engineering and Computers at Coimbra, Coimbra, Portugal
[10]Hematology Clinic Department, Centro Hospitalar Universitário de Coimbra, Coimbra, Portugal
[11]Immunology Institute, Faculty of Medicine, University of Coimbra, Coimbra, Portugal
*Corresponding author: fjmendes@estescoimbra.pt

Abstract **Background**: Diffuse large B cell lymphoma (DLBCL) is recognized as a heterogeneous group of hematological malignancies, and collectively forms the most common type of aggressive, non-Hodgkin lymphoma. The aim of our study was to evaluate the cellular and molecular effects of high doses X radiation in a DLBCL cell line. **Materials and Methods:** Farage cells were cultured and exposed to 0.5-60 Gy of Ionizing Radiation (IR). Cell viability and proliferation were assessed by trypan blue assay. Cell survival was determined with clonogenic assay. Cell death was assessed by flow cytometry (FC) and by optical microscopy. Cell cycle, mitochondrial membrane potential, reactive oxygen species, GSH and BAX/BCL-2 ratio were measured by FC. DNA damage was evaluated using comet assay. Total and phosphorylated P53 was assessed by western blot. **Results:** IR induced cytotoxic and cytostatic effects in Farage cells in a dose and time dependent manner with an LD50 of 1.73 Gy. Cell death occurs mainly by apoptosis or later apoptosis/necrosis with an increase in BAX/BCL-2 ratio and a significant increase in ROS production. We also observed cell cycle arrest at G_2/M phase and a significant increase in DNA damage as well as P53 total and phosphorylated expression levels. **Conclusions:** High doses of IR induces a time and dose dependent response which leads to increased ROS production, DNA damage with the increased P53 expression and activation expressed by elevated levels of pP53, resulting in G_2/M cell cycle arrest and increases in later apoptosis/necrosis cell death. Our results showed that single shot IR induces effects in different cell components and its comprehension is essential to choose the treatment planning.

Keywords: *large diffuse B cell lymphoma, radiotherapy, genotoxicity, oxidative stress, cell death, P53*

Cite This Article: Fernando Mendes, Cátia Domingues, Susann Schugk, Ana Margarida Abrantes, Ana Cristina Gonçalves, Tiago Sales, Ricardo Teixo, Rita Silva, Jéssica Estrela, Mafalda Laranjo, João Casalta-Lopes, Clara Rocha, Paulo César Simões, Ana Bela Sarmento, Maria Filomena Botelho, and Manuel Santos Rosa, "Single Shot Irradiation and Molecular Effects on a Diffuse Large B Cell Lymphoma Cell Line." *Journal of Cancer Research and Treatment*, vol. 4, no. 1 (2016): 9-16. doi: 10.12691/jcrt-4-1-2.

1. Introduction

Diffuse large B cell lymphoma (DLBCL) is recognized as a heterogeneous group of hematological malignancies, and collectively forms the most common type of aggressive, non-Hodgkin lymphoma (NHL) [1].

Within largest category, DLBCL, not otherwise specified, gene expression profiling (GEP) studies have identified two distinct molecular subtypes, termed germinal center B cell (GCB) and activated B cell (ABC), although 15 % of patients remaining unclassifiable, which are believed to represent lymphomas arising from different stages of lymphoid differentiation [2,3]. Standard treatment of NHL involves chemotherapy based on the combination of cyclophosphamide, doxorubicin, vincristine, prednisone and monoclonal antibody anti-CD20 (rituximab) (R-CHOP), and complementary radiotherapy (RT) [1].

Radiotherapy as part of the therapy has been controversial and lively debated during past decades.

Recent guidelines [4] emphasise RT as an important complement to chemotherapy, regardless tumour stage and presence of bulky events. R-CHOP treatment has proven to provide very effective results in limited or advanced stage of disease. However, treatment solely involving R-CHOP submits patients to chemotherapy-induced toxicities, which may be avoided with RT [1]. Radiation doses used for patients with a variety of lymphoma histologies have been reduced over last decade. A randomized study from UK demonstrated no difference between applying RT in a dose of 30 vs 45 Gy in patients with DLBCL [5]. For stage I/II, a dose of 30 Gy is currently considered standard therapy in the setting of a negative PET scan post-chemotherapy [6]. RT produces very high local complete response rates for all lymphoma subtypes and given this high clinical efficacy, it is not surprising that RT has played an important part in curative treatment of a broad range of lymphomas over the past half century [7].

Different forms of RT, such as involved field radiation therapy (IFRT), involved nodal radiation therapy (INRT) or involved site radiotherapy (ISRT) with R-CHOP improve prognostic outcomes and overall survival rates. The different RT methods alone may be used in chemotherapeutic unresponsive patients or who developed adverse effects. The establishment of radiotherapy as a possible treatment strategy in DLBCL could provide beneficial prognostic advantage in early stage or localized disease.

Ionizing radiation (IR) induces direct and indirect cell effects, namely single and double strand breaks in DNA, sister-chromatide exchanges, micronucleation, mutations, gene expression alterations, oxidative stress (OS) and apoptosis. Many tumors show an increased expression of antioxidant molecules, which could enhance the RT resistance in tumor cells by neutralizing oxygen reactive species, being this one of the major problems associated with RT failure [1]. Moreover, OS effects may be mediated by mitochondria dysfunction and/or alternation of P53 expression levels. However, a better understanding of these molecular mechanisms can help to overcome these problems. Thus, the aim of our study was to evaluate and characterize cellular and molecular effects of single shot doses of X radiation in a DLBCL cell line.

2. Materials and Methods

2.1. Cell Lines

DLBCL Farage cell line (ATCC® CRL-2630™) was cultured in Roswell Park Memorial Institute medium (RPMI) 1640 supplemented with 10% fetal bovine serum (FBS, Sigma, USA), 1% penicillin-streptomycin (GIBCO 15140-122, UK) at 37ºC with 5% CO_2 in a humidified incubator. For all experiments cells were plated at a density of $0.5x10^6$ cells/ml.

2.2. Irradiation

Cell suspensions were exposed to IR (0.5–60 Gy) in a Varian 600C Linear Accelerator 12D10 (LINAC, Radiology Oncology Systems Inc., USA), a low photon energy radiator delivering high energy photon beams. The energy interval of LINAC ranged between 1-50 MeV. For samples irradiation photons of 4 MeV was used. Standards of the International Code of Practice for Dosimetry, TRS-398, published by International Atomic Energy Agency were assumed as references for calibration and dose calculations [8]. The device allows administration of 50-250 monitor units (MU)/minute and 1 MU corresponds to 0.022 Gy [8,9]. Dose administration was cumulative and applied from two different angles (90^o and 270^o) to ensure conformity field (Table 1). For clonogenic assay, cells were irradiated with 0.5 Gy, 2 Gy, 5 Gy, 8 Gy, 12 Gy, 15 Gy, 30 Gy, and 60 Gy. For all other experiments cells were irradiated with 0.5 Gy, 15 Gy, 30 Gy, and 60 Gy.

2.3. Cell Viability and Proliferation Assay

Cell viability and proliferation were assessed by trypan blue exclusion assay, as described previously [10]. During 96 h, cells were harvest and number of stained (nonviable) and unstained (viable) cells were counted using a Neubauer chamber, each 24 h. Viability was calculated as percentage of viable cells and cell proliferation was determinate by number of viable cells (density).

2.4. Clonogenic Assay

Cell suspensions were irradiated with different doses and then plated into six well plates and incubated as described above. After 7 days, cells were fixed, stained with crystal violet (0.4% in methanol) and counted. Survival factor (SF) was calculated [11,12,13].

2.5. Evaluation of Cell Death and Mechanisms of Cell Death

Farage cells were exposed to IR and 48h after, cell death was assessed by morphological May-Grünwald-Giemsa stained slides and flow cytometry (FC) using annexinV (AnV) and propidium iodide (PI) double staining [14,15]. For morphological assessment, cells were transferred to slides, fixed, stained and evaluated under light microscopy, using a Nikon Eclipse 80i equipped with a Nikon Digital Camera DXm 1200F. For flow cytometry assessment, AnV/PI double staining were performed according to manufacturer's protocol (Annexin V-FITC Apoptosis Detection Kit, Immunostep, Spain). Briefly, $0.5x10^6$ cells/ml were washed in ice-cold phosphate buffer saline (PBS), centrifuged at 500xG, 5 min, suspended in AnV binding buffer and incubated with AnV fluorescein isothiocyanate (FITC) conjugated and PI. After 15 min in dark, cells were diluted in 400 µl of binding buffer, and analyzed in a six parameter, four color FACSCalibur flow cytometer (Becton Dickinson, San Jose, CA, USA) equipped with an argon laser 15 nW. For each test, $1x10^6$ cells were used and data on at least 10,000 events was obtained using Cell Quest Software (Becton Dickinson) and analyzed by means of Paint-a-Gate software (Becton Dickinson).

BAX and BCL-2 expression levels were analyzed by FC and BAX/BCL2 ratios were calculated [14]. Briefly, $0.5x10^6$ cells/ml were incubated with monoclonal antibodies anti-BAX conjugated with phycoerythrin (PE) (Santa Cruz Biotechnology Inc.) and anti-BCL-2 conjugated with

FITC (Santa Cruz Biotechnology Inc.), according to manufacturer's protocol.

Mitochondrial membrane potential (MMP) was evaluated using the 5.5′.6.6′-tethrachloro-1.1′.3.3′-tetraethylbenzimidazolcarbocyanine iodide (JC-1) (Molecular Probes, Invitrogen, USA) [10,14]. Succinctly, $0.5x10^6$ cells/ml were washed with PBS, centrifuged at 300xG, 5 min, and incubated with 5 µg/ml of JC-1, 15 min at 37°C in dark. After, cells were washed with PBS and analyzed by FC. Results are expressed as monomers (M)/aggregates (A) ratio.

2.6. Cell cycle Analysis

For cell cycle analysis, $0.5x10^6$ cells/ml were washed with PBS, centrifuged at 500xG, 5 min and fixed in 70% ethanol at 4°C, 30 min in dark. After, cells were washed in PBS and incubated with PI/RNase solution (PI/RNase, Immunostep, S.L., Salamanca, Spain) 15 min, in dark [14,16]

2.7. Oxidative Stress Evaluation

Oxidative stress was evaluated trough reactive oxygen species (ROS) production and anti-oxidative defenses, with 2′,7′-dichlorodihydrofluorescin diacetate (H_2DCF-DA), dihydroethidine (DHE), and mercury orange. Briefly, $0.5x10^6$ cells/ml were incubated with 5 µM of $DCFH_2$-DA (Molecular Probes, Invitrogen, USA), 30 min, with 2 µM of DHE (Sigma-Aldrich, USA), 15 min, or with 40 µM of mercury orange (Sigma, EUA), 15 min, at 37°C in dark. Cells were washed with PBS, and fluorescence was detected by FC [11,17,18].

2.8. Total and Phosphorylated P53 Expression Evaluation

Total and phosphorylated P53 were evaluated by western blot analysis according to standard protocol [12]. Briefly, 48 h after radiation exposure, total protein extracts were prepared on ice using a radioimmunoprecipitation assay (RIPA) buffer supplemented with cOmplete Mini (Roche) for total P53 evaluation and with PhosphoStop® (Roche) for phosphorylated P53. After sonication and centrifugation with 14,000xG, samples were kept at -80ºC. Protein content was determined by bicinchoninic acid method. Sodium dodecyl sulfate polyacrylamide gel electrophoresis (SDS-PAGE) was performed in 10% acrylamide gel, 20 min at 80 V followed by 160 V till 90 min. Subsequently proteins were electrotransferred at 100 V during 1 h to nitrocellulose (PVDF) membranes. PVDF membranes blocking was performed with 5% bovine serum albumin in tris-buffered saline tween-20 (TBS-T). 1 h at room temperature with stirring. Incubation with primary antibodies against total P53 (1:200) (P53 DO-7; Sc47698 Santa Cruz Biotechnology, California, USA), phosphorylated P53 (1:100) (P53-18; sc-13580, Santa Cruz Biotechnology, California, USA) and β-actin (1:10,000) (Anti-β-Actin mouse monoclonal antibody, A5441, Sigma, USA) was performed overnight at 4ºC. After several washes with TBS-T, membranes were incubated with secondary antibody (1:10,000) (anti-mouse antibody) for 1 h at room temperature and subsequently washed again. Finally the blots were stained with fluorescent dye and reading in a 9000 Typhoon FLA equipment. Quantification of fluorescence was performed by ImageQuant Software (GEHealthcare).

2.9. Comet Assay

DNA damage was analyzed with alkaline single-cell gel electrophoresis, comet assay 48 h after radiation exposure [12,19]. As positive control cells were incubated with 20 nM of hydrogen peroxide (Sigma Aldrich®, EUA), 15 min at 4°C. Controls and treated cells were collected and counted to prepare a suspension with 5×10^4 cell/ml. Cell suspensions were diluted 1:1 in 1% low melting point agarose and applied in slides previously overlaid with 1% normal melting point agarose. Slides were submerged in alkaline lysis solution (2.5 M NaCl, 100 mM EDTA, 10 mM Tris, 10% DMSO and 1% Triton x-100, Sigma Aldrich®, EUA) overnight. Slides were equilibrated in alkaline electrophoresis buffer (300 mM NaOH and 1 mM EDTA, pH > 13) and then submitted to 25 V and 1 A, 5 min. After electrophoresis, slides were incubated in neutralizing buffer (0.4 M Tris, pH 7.4) 3 times, 5 min each, and stained with 25 µg ml^{-1} ethidium bromide, for 20 min. Slides were washed in distilled water and visualized in a fluorescent inverted microscope with a 100W mercury lamp which excitation wavelength was 546 nm with an emission of 580/10 nm. Image acquisition was performed with the software Motic Images 2.0 (Microscope world, EUA).

2.10 Statistical Analysis

All results are expressed as a mean ± standard error (SEM) of a minimum of four independent experiments. Statistical analysis was performed using software IBM SPSS® v.19 (National Opinion Research Center, Chicago, USA). To evaluate the normality of distribution of variables Shapiro-Wilk test was used. When distribution was normal parametric tests were used, otherwise non parametric tests were used. Comparison of results was performed using Mann-Whitney test (non parametric test). Comparison of the qualitative variables between more than two groups was obtained using Kruskal-Wallis (non parametric test) or using the ANOVA 1 Fixed Factor test (parametric test). Multiple comparisons were performed considering Bonferroni correction. Comparison of results of clonogenic assays with respective control was performed by determination of 95% confidence range, considering significant when this value did not include the value 1.

3. Results

3.1. Viability, Proliferation and Survival

Farage cells exposed to IR decreased viability and proliferation depending of dose and time, as shown in Figure 1. Viability, after exposure, decreased significantly ($P<0.05$ for 0.5 Gy and $P<0.001$ for 15, 30 and 60 Gy) for all doses tested and half inhibitory dose was about 30 Gy, as seen in Figure 1A. Behaviour of proliferation along time and with radiation doses was different. With 0.5 Gy, a modest cell growth during the first 24 hours was observed, that is maintained for all times considered. For other doses (15, 30 and 60 Gy) a continuous and

significant (P<0.001) decrease was observed for all times comparing to controls (Figure 1B).

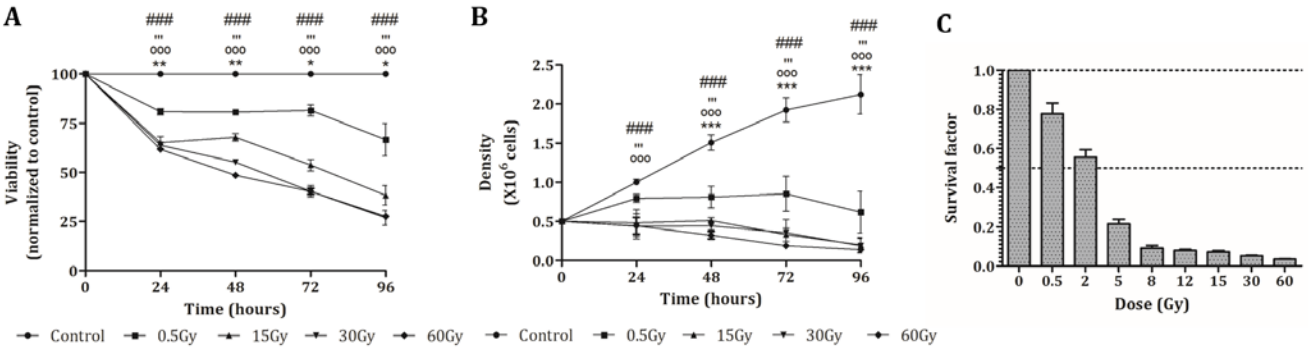

Figure 1. Cell viability, proliferation and survival

Figure 1 – Farage cell viability (A), proliferation (B) and survival (C) after exposure to IR. (A) Dose-response curves and (B) cell proliferation of Farage cells obtained by Trypan Blue exclusion assay, assessed 24h, 48h, 72h and 96h after IR exposure. Results are expressed as percentage of viability, normalized to control, and as cell density (number of viable cells), respectively. (C) Representation of survival factor assessed by clonogenic assay 7 days after exposure to IR. Results are normalized to control as mean±SEM of at least six independent experiments. Statistical significance is represented for each dose in relation to control: 0.5 Gy; ***P<0.001; 15 Gy °P<0.05; °°P<0.01; °°°P<0.001; 30 Gy ‘P<0.05; ‘’P<0.01 ‘’’ P<0.001); 60 Gy $^{\#}P$<0.05, $^{\#\#}P$<0.01; $^{\#\#\#}P$<0.001.

Related to survival factor (SF), all doses significantly reduced it, depending of dose. The median lethal dose (LD_{50}) was 1.73±0.27 Gy calculated applying the linear-quadratic model.

3.2. Cell Death

Cell death was evaluated trough different methodologies in order to understand what are the mechanisms involved, 48 hours after radiation exposure (Figure 2).

Morphological features of Farage cells stained with May-Grünwald-Giemsa are showed in Figure 2A. Morphologic studies demonstrated that exposure to lower IR doses induced an increase in number of cells undergoing morphological characteristics of apoptotic cell death, such as blebbing, chromatin condensation, nuclear fragmentation and apoptotic bodies (Figure 2A-B and A-C). Moreover, exposure to higher doses showed an increased number of cell undergoing necrosis, as observed in Figure 2A-D and Figure 2A-E.

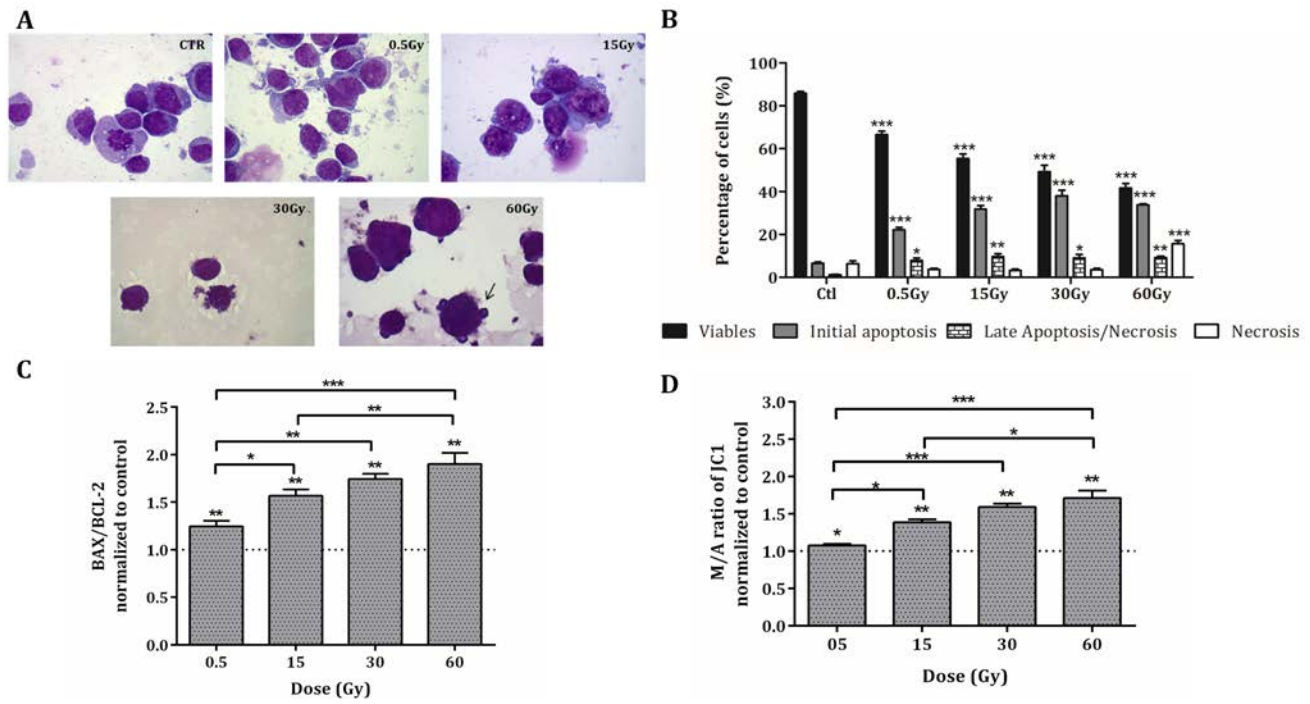

Figure 2. Cell death mechanisms

Figure 2 – Evaluation of Farage cell death induced by ionizing radiation. (A) Assessment of morphologic features of Farage cells by May-Grunwald-Giemsa staining after IR exposure. Representative images of Control, 0.5 Gy, 15 Gy, 30 Gy, and 60 Gy. Arrows represent the formation of *blebbings*. Amplification 400X. (B) Cell viability and types of cell death of Farage cells 48h after IR exposure assessed by flow cytometry by Annexin V/Propidium Iodide double staining. Results are expressed as mean±SEM of percentage of viable cells and cells undergoing cell death by initial apoptosis, late apoptosis/necrosis and necrosis, of at least four independent experiments. (C) Assessment of BAX/BCL-2 ratio 48h after IR exposure. (D) Evaluation of mitochondrial membrane potential 48h after IR exposure, assessed by flow cytometry using JC-1. Results are expressed as mean±SEM of mean intensity fluorescence normalized to control of at least four independent experiments. Statistical significance is expressed in relation to control as: P<0.05, **P<0.01 e ***P<0.001.

FC results using AnV/PI double staining showed that IR significantly decreases Farage cells viability in a dose dependent manner, as we can observe in Figure 2B, comparing to control cells (85.80±0.92%) exposure to 0.5

Gy (66.50±1.73%, *P*<0.001), 15 Gy (55.40±2.14%, *P*<0.001), 30 Gy (49.20±3.09%, *P*<0.001) and 60 Gy (41.60±2.16%, *P*<0.001) decreased cell viability. Moreover, once IR reduced the number of viable cells, we can observe an increase in apoptotic population compared to control (6.60±0.51%), namely for 0.5 Gy (22.17±1.14%, *P*<0.001), 15 Gy (31.80±1.66%, *P*<0.001), 30 Gy (38.00±2.65%, *P*<0.001) and 60 Gy (33.80±0.58%, *P*<0.001). We also observed a significant increase in late apoptotic/necrotic cell population compared to control (1.20±0.20%) to 0.5 Gy (7.83±1.19%, *P*=0.038), 15 Gy (9.60±1.44%, *P*=0.009), 30 Gy (9.00±1.70%, *P*=0.029) and 60 Gy (9.20±0.66%, *P*=0.0013).

To evaluate some mechanisms of IR apoptosis modulating, BAX/ BCL-2 ratio was analysed by FC. As observed in Figure 2C, increasing doses of IR significantly increased BAX/BCL-2 ratio compared to control: 0.5 Gy (1.24±0.06, *P*=0.014), 15 Gy (1.57±0.07, *P*=0.001), 30 Gy (1.75±0.05, *P*=0,001) and 60 Gy (1.90± 0.12, *P*=0,005).

Moreover, to confirm mitochondrial involvement in cell death induced by IR exposure, MMP was evaluated by FC using JC1 dye. In apoptotic cells, mitochondrial membrane potential collapses, and JC-1 cannot accumulate within the mitochondria, remaining in the monomeric form in cytosol. We observed an increased M/A of JC1 proportional to increasing doses of IR, reflecting a decrease in MMP. Thus, as depicted in Figure 2D, MMP increases with exposure to radiation doses of 0.5 Gy (1.07±0.002, *P*=0.045), 15 Gy (1.39±0.04, *P*=0.002), 30 Gy (1.59±0.04, *P*=0.001) and 60 Gy (1.71±0.10, *P*=0.006).

3.3. Cell cycle and Oxidative Stress

As IR induced antiproliferative effects, we assessed distribution of Farage cells in cell cycle. The results obtained are illustrated in Figure 3A. We observed, 48h after IR exposure, a significant increase in pre-G_0/G_1 peak between control (2.60±0.51%) and 15 Gy (12.50±1.57%, *P*<0.001), 30 Gy (19.33±0.99%, *P*<0.001) and 60 Gy (12.25±1.60%, *P*<0.001). We also observed a significant decrease in G_0/G_1 phase compared to control (64.20±1.6%) and 15 Gy (31.00±1.93%; *P*<0001), 30 Gy (32.33±2.39%, *P*<0.001) and 60 Gy (41.50±0.96%, *P*<0.001). There was a significant cell cycle arrest in G_2/M phase after IR exposure, comparing to control (10,40±1,72%) for the doses of 15 Gy (29.00±3.54%, *P*<0.001), 30 Gy (25.33±3.54%, *P*<0.001) and 60 Gy (42.25±2.75%, *P*<0.001).

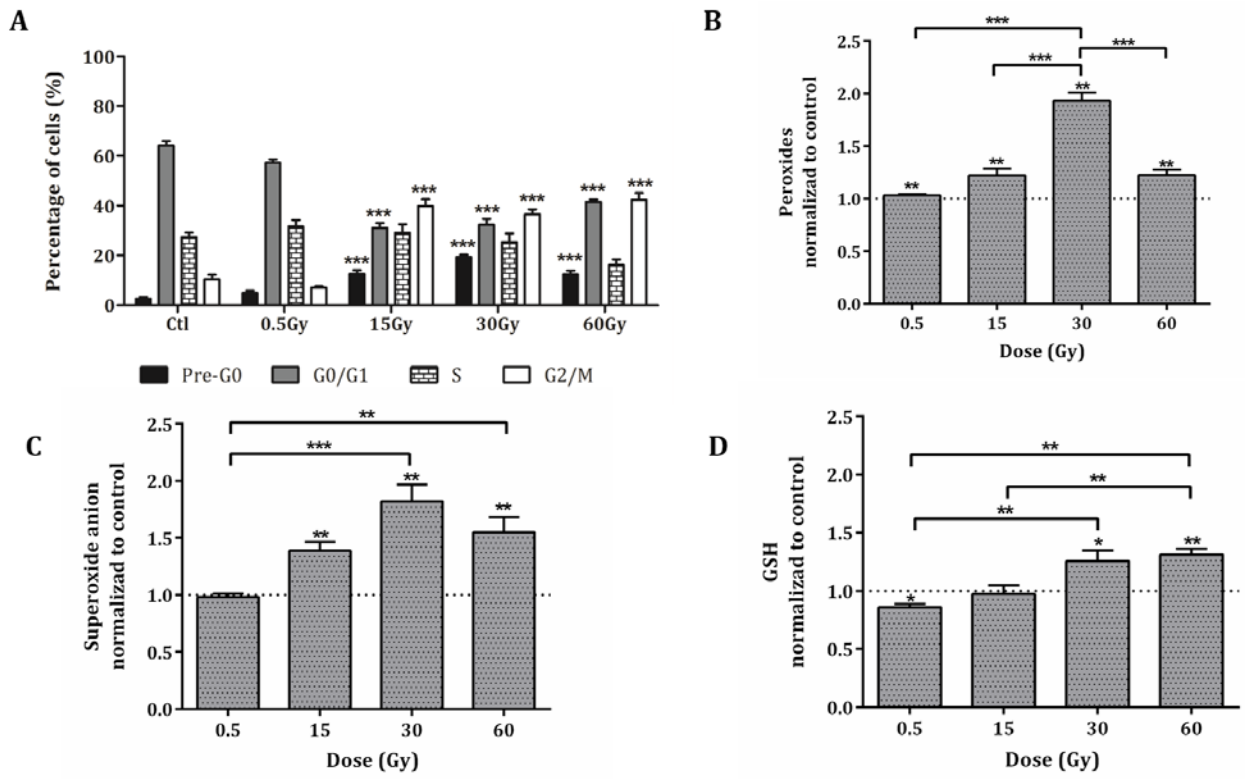

Figure 3. Cell cycle and oxidative stress alterations

Figure 3 – Evaluation of cell cycle and oxidative stress alterations after IR exposure on Farage cells. (A) Assessment of cell cycle by flow cytometry and graphic representation of phases of cell cycle in Farage cells. Results are expressed as mean±SD of percentage of cells identified for each phase of cell cycle of at least four independent experiments. Assessment of oxidative stress by flow cytometry by evaluation of intracellular levels of peroxides (B), superoxide anion (C) and GSH (D) in Farage cells. Results are expressed as mean intensity of fluorescence as mean±SEM of at least four independent experiments. Statistical significance is expressed in relation to control: *P<0,05, **P<0,01 e ***P<0,001.

Moreover, ROS levels (peroxides and $O_2^{\cdot}$) were determined using the probes DCFH-DA and DHE, respectively, as well as the antioxidant defence GSH. Generally, as showed in Figure 3B, ROS production significantly increases after IR exposure. In fact, significant increase of peroxides was observed compared to control for the doses of 15 Gy (1.22±0.07, *P*=0.043), 30 Gy (1.93±0.08, 0.001) and 60 Gy (1.22±0.05, 0.024). Similar results were observed for superoxide anion, with a significant increase compared to control for the doses of 15 Gy (1.39±0.08, *P*=0.016), 30 Gy (1.82±0.15, *P*=0.011) and 60 Gy (1.55±0.13, *P*=0.024). GSH levels also showed a significant increase for the dose of 30 Gy (1.26±0.09, *P*=0.046) and 60 Gy (1.31±0.05, *P*=0.004), as showed in Figure 3B.

3.4. DNA Damage

IR is usually related with mono and/or bis-alkylation of DNA and consequently to cell death. According to Figure 4A, we observed increased and more pronounced number of comet after 30 Gy of IR exposure. We also observed a significant increase of tail moment compared to control for doses of 15 (P<0.001), 30 Gy (P<0.001) and 60 Gy (P<0.001), as showed in Figure 4B.

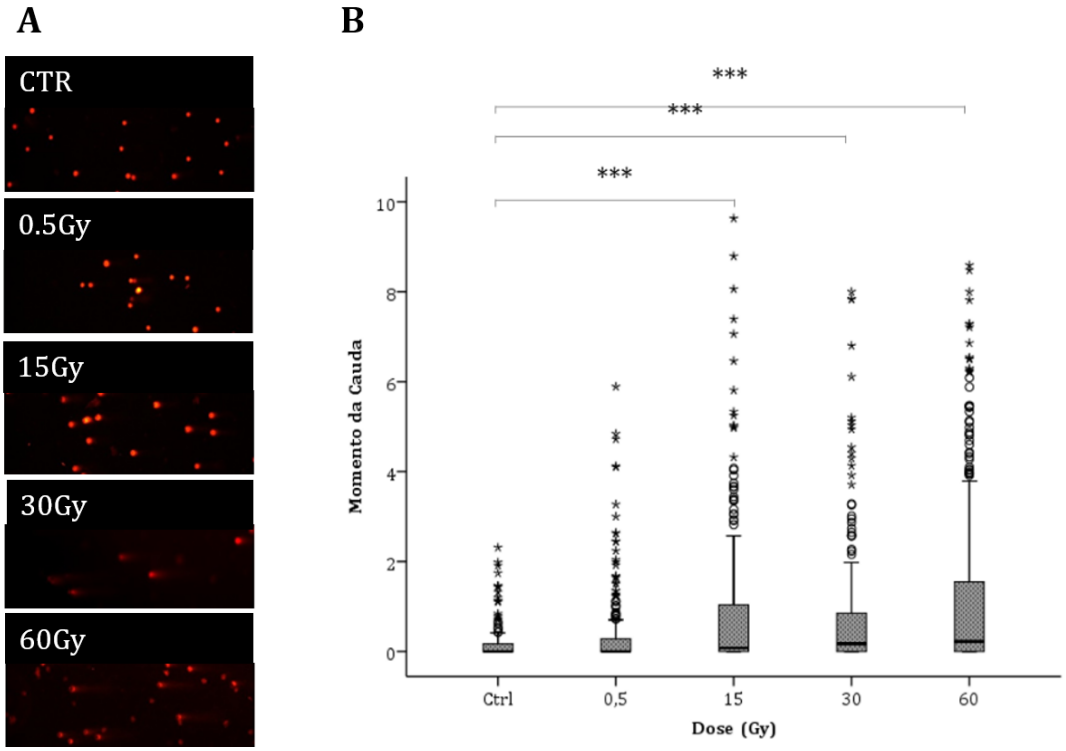

Figure 4. Genotoxicity

Figure 4 – Genotoxicity induced in Farage cells after IR exposure. (A) Illustrative photographies of single cell gel electrophoresis (comet assay) in DLBCL cell line Farage, 48h after exposure to IR with the doses of 0.5 Gy, 15 Gy, 30 Gy, 60 Gy and control (CTR). (B) Representation of tail moment determined by comet assay 48h after IR exposure. Results are expressed as mean±SD of six independent experiments (n=6), with a minimum of 100 comets for each condition. Statistical significance is expressed in relation to control: ***P<0.001

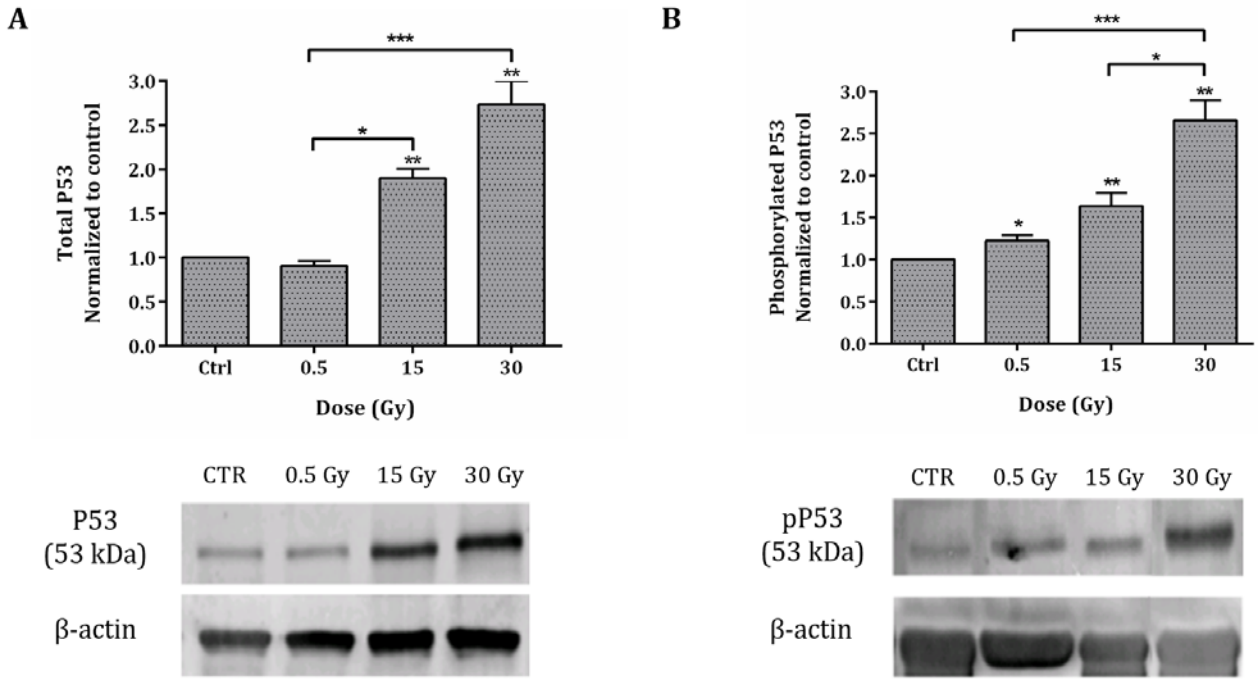

Figure 5. P53 and pP53

Figure 5: Expression of total P53 (A) and phosphorylated P53 (B) in Farage cells, 48h after exposure to IR. Results are expressed as mean intensity of fluorescence of total P53/actin ratio (A) and pP53/actin ratio (B) normalized to control after exposure to 0.5 Gy, 15 Gy and 30 Gy. Graphics represent mean±SEM of four independent experiments while images are representative immunoblots of expression of total P53 and pP53 and β-actin for each experimental condition. Statistical significance is represented in relation to control: P<0.05; ** P<0.01.

3.4. P53 Expressions

P53 protein plays a key role in regulation of multiple cellular steps, alterations in this protein disrupt normal cell regulation. As we can observed in Figure 5A, IR induces a significant increase in total P53 expression levels compared to control for the doses of 15 Gy (1.90±0.11, *P*=0,001) and 30 Gy (2.74±0.26, *P*=0.001). Moreover, phosphorylated P53 levels increased in Farage cells compared to control when cells were exposure to IR for all doses (0.5 Gy (1.22±0.07, *P*=0.044), 15 Gy (1.64±0.16, *P*=0.007) and 30 Gy (2.66±0.24, *P*=0.006)), as described in Figure 5B.

4. Discussion

Radioresistance stands as a fundamental barrier that limits effectiveness of RT in cancer treatment. Recent evidences suggest that radioresistance is due to tumor repopulation and involves several signaling pathways. Thus, by better understanding cellular and molecular mechanisms induced by IR may contribute, in the near future, to reduce the number of cases of radiorresistance [1]. Although RT is being slowly phased out by other treatment strategies, including chemotherapy, it is still a highly important treatment. Establishment of RT as a possible treatment strategy in DLBCL could provide beneficial prognostic advantage in early stage or localized disease [1]. To date, completion of radiotherapy treatment, using high single doses, was not extensively studied, partly due to recent innovations in irradiation devices and at planning and use of three-dimensional functional image that begin to be used in treatment regimens [1]. Thus, it becomes essential to study RT, evaluating proliferation, viability, type of induced death and injury to DNA of cells exposed to different single doses of IR.

Our results showed that IR induces cytotoxic and antiproliferative effects in Farage cells in a dose and time dependent manner. However, these results give us a short time evaluation of IR effect, and clonogenic assay is the gold standard for long time survival. Thus, we verified that LD50 for Farage cells is 1,73±0,61 Gy which is low, compared to other cell lines, namely in solid tumors such as A549 and H460 cells, using a dose rate of 70.6 rad/min at room temperature [20], and compared with results obtained by us in a study concerning three lung cancer cell lines [14]. In fact, IR induces activation of multiple intracellular mechanisms such as DNA damage, cell cycle arrest and ROS production [14]. We observed that the mechanism that IR induced cell death in Farage cells is dose dependent, inducing cell death mainly by apoptosis, as observed by increased cell populations in apoptotic cell death and increased BAX/BCL-2 and M/A ratios. This results were also observed by us in $P53^{Wild}$ A549 cells [14]. These results may be related to significant increased ROS production, namely by increased superoxide anion and H_2O_2 which was also evaluated by other authors [21–23]. Moreover after IR exposure, Farage cells tried to recover from the imbalance in oxidative environment by increasing GSH levels significantly. Other authors provided evidence for two distinct phases of ROS generated following IR exposure, one that reveled a late ROS increase associated with reduced GSH, and MMP and another related to exogenous ROS that induces cytochrome *c* release directly in isolated mitochondria which indicates that late ROS production is associated with critical mitochondrial functions, likely to be tightly linked to caspase activation and cytochrome *c* release [24]. We observed that participation of mitochondria pathway is also regulated by a tight balance between pro-apoptotic BAX and anti-apoptotic BCL-2 which are crucial to IR mechanism [14,25].

IR exposure also induced cell cycle arrest in Farage cells at G_2/M phase, which may be related with significant increased ROS production and DNA damage followed by great and concomitant increase in total P53 and in pP53, which plays a key role in apoptosis regulation and cell cycle arrest, as we had observed in A549 lung cancer cells [14]. Indeed, P53 activation is well known to regulate apoptotic cell death, after exposure to cellular insults, including DNA damage, oncogene activation or hypoxia [26,27,28]. After DNA injury, $P53^{wild}$ is activated promoting cell cycle arrest, transactivation of repairing enzymes and, if damage cannot be repaired, apoptosis [26,27,28]. Due to its alterations, such as mutations and altered expression, P53 promotes growth advantage and ensures survival in cancer cells by inhibiting apoptotic response necessary for tumor suppression [23,29,30]. Montero *et al*. (2013) showed that P53 can also control non-apoptotic cell death and it may be selected by cancer cells to provide not only their resistance to apoptosis but also to necrosis, and this mechanism may explain resistance to chemo and radiotherapy even when leading to non-apoptotic mechanisms [26].

In summary, our results showed that IR induces cell death in a time and dose dependent manner. The study of type of cell death and underlying mechanisms in these cells revealed that IR in Farage cells induces damage that leads to intrinsic apoptotic cell death. On this way, cell death occurs preferential by apoptosis or later apoptosis/necrosis with significant increase in ROS production, DNA damage leading to increased expression and activation of P53, resulting in G_2/M cell cycle arrest. Our results showed that IR effects can alter a significant number of cellular and molecular targets and that its comprehension is essential to highlight the importance of IR on DLBCL treatment.

Acknowledgments

The authors would like to thank the Portuguese Foundation for Science and Technology for the financial support (Strategic Project PEst-C/SAU/UI3282/2013 and UID/NEU/04539/2013, COMPETE-FEDER) and to Radiotherapy Service of the Centro Hospitalar e Universitário de Coimbra.

Conflict of Interest Statement

The authors declare that they have nothing to disclose.

References

[1] Mendes F, Domingues C, Teixo R, Abrantes AM, Gonçalves AC, Nobre-Gois I, et al. The importance of radiotherapy on diffuse

large B cell lymphoma treatment: a current review. *Cancer Metastasis Rev*, 34 (3):511-25, September, 2015.

[2] Zelenetz AD, Wierda WG, Abramson JS, Advani RH, Andreadis CB, Bartlett N, et al. Non-Hodgkin's lymphomas, version 1.2013: Featured updates to the NCCN guidelines. *JNCCN J Natl Compr Cancer Netw*, 11: 257-273, March, 2013.

[3] Tilly H, Dreyling M. Diffuse large B-cell non-Hodgkin's lymphoma: ESMO Clinical Practice Guidelines for diagnosis, treatment and follow-up. *Ann Oncol*, 21 (5): 172-174, Mat, 2010.

[4] Boyle J, Beaven AW, Diehl LF, Prosnitz LR, Kelsey CR. Improving Outcomes in Advanced DLBCL: Systemic Approaches and Radiotherapy. *Oncology*, 28 (12): 1074-1081, December, 2014.

[5] Wirth A. The rationale and role of radiation therapy in the treatment of patients with diffuse large B-cell lymphoma in the Rituximab era. *Leuk Lymphoma*, 48: 2121-2136, November 2007.

[6] Illidge T, Tolan S. Current treatment approaches for diffuse large B-cell lymphoma. *Leuk Lymphoma*, 49: 663-676, April, 2008.

[7] Illidge T. X. When should radiotherapy be used in lymphoma? *Ann Oncol*, 22: 57-60, June, 2011.

[8] Andreo P, Burns DT, Hohlfeld S, Huq MS, Kanai T, Laitano F, et al. Absorbed Dose Determination in External Beam Radiotherapy: An International Code of Practice for Dosimetry based on Standards of Absorbed Dose to Water. vol. 2011. IAEA. Vienna, Austria: 2011.

[9] Gibbons JP. Monitor Unit Calculations for External Photon and Electron Beams. AAPM Annu. Meet. Refresh. Course, Salt Lake City: 2001, 1-10.

[10] Gonçalves AC, Alves V, Silva T, Carvalho C, Oliveira CR De, Sarmento-Ribeiro AB. Oxidative stress mediates apoptotic effects of ascorbate and dehydroascorbate in human Myelodysplasia cells in vitro. *Toxicol Vitr*, 27: 1542-1549, August, 2013.

[11] Mamede AC, Pires AS, Abrantes AM, Tavares SD, Gonçalves AC, Casalta-Lopes JE, et al. Cytotoxicity of ascorbic acid in a human colorectal adenocarcinoma cell line (WiDr): in vitro and in vivo studies. *Nutr Cancer*, 64: 1049-1057, September, 2012.

[12] Santos K, Laranjo M, Abrantes AM, Brito AF, Gonçalves C, Sarmento Ribeiro AB, et al. Targeting triple-negative breast cancer cells with 6,7-bis(hydroxymethyl)-1H,3H-pyrrolo[1,2-c] thiazoles. *Eur J Med Chem*, 79: 273-281, May, 2014.

[13] Franken N a P, Rodermond HM, Stap J, Haveman J, van Bree C. Clonogenic assay of cells in vitro. *Nat Protoc*, 1: 2315-2319, 2006.

[14] Mendes F, Sales T, Domingues C, Schugk S, Abrantes AM, Gonçalves AC, et al. Effects of X-radiation on lung cancer cells: the interplay between oxidative stress and P53 levels. *Med Oncol*, 32 (12): 266-274, 2015.

[15] Gonçalves AC, Barbosa-Ribeiro A, Alves V, Silva T, Sarmento-Ribeiro AB. Selenium Compounds Induced ROS-Dependent Apoptosis in Myelodysplasia Cells. *Biol Trace Elem Res*, 154: 440-447, September, 2013.

[16] Serra AC, Rocha Gonsalves AMD a, Laranjo M, Abrantes AM, Gonçalves AC, Sarmento-Ribeiro AB, et al. Synthesis of new 2-galactosylthiazolidine-4-carboxylic acid amides. Antitumor evaluation against melanoma and breast cancer cells. *Eur J Med Chem*;53: 398-402, July, 2012.

[17] Laranjo M, Serra AC, Abrantes M, Piñeiro M, Gonçalves AC, Casalta-Lopes J, et al. 2-Bromo-5-hydroxyphenylporphyrins for photodynamic therapy: photosensitization efficiency, subcellular localization and in vivo studies. *Photodiagnosis Photodyn Ther*, 10: 51-61, February, 2013.

[18] Almeida S, Sarmento-ribeiro AB, Januário C, Rego AC, Oliveira CR. Evidence of apoptosis and mitochondrial abnormalities in peripheral blood cells of Huntington' s disease patients. *Biochem Biophys Res Commun*, 374: 599-603, October, 2008.

[19] Olive PL, Banáth JP. The comet assay: a method to measure DNA damage in individual cells. *Nat Protoc*, 1: 23-29, 2006.

[20] Gomez-Casal R, Bhattacharya C, Ganesh N, Bailey L, Basse P, Gibson M, et al. Non-small cell lung cancer cells survived ionizing radiation treatment display cancer stem cell and epithelial-mesenchymal transition phenotypes. *Mol Cancer*, 12: 94-106, August, 2013.

[21] Yamaguchi M, Kashiwakura I. Role of reactive oxygen species in the radiation response of human hematopoietic stem/progenitor cells. *PLoS One*, 8 (7): e70503, July, 2013.

[22] Lee JH, Kim SY, Kil IS, Park J-W. Regulation of ionizing radiation-induced apoptosis by mitochondrial NADP+-dependent isocitrate dehydrogenase. *J Biol Chem*, 282: 13385-13394, May, 2007.

[23] Yamamori T, Yasui H, Yamazumi M, Wada Y, Nakamura Y, Nakamura H, et al. Ionizing radiation induces mitochondrial reactive oxygen species production accompanied by upregulation of mitochondrial electron transport chain function and mitochondrial content under control of the cell cycle checkpoint. *Free Radic Biol Med*, 53: 260-270, July, 2012.

[24] Chen Q, Chai Y-C, Mazumder S, Jiang C, Macklis RM, Chisolm GM, et al. The late increase in intracellular free radical oxygen species during apoptosis is associated with cytochrome c release, caspase activation, and mitochondrial dysfunction. *Cell Death Differ*, 10: 323-334, March, 2003.

[25] Loriot Y, Mordant P, Dugue D, Geneste O, Gombos A, Opolon P, et al. Radiosensitization by a novel Bcl-2 and Bcl-XL inhibitor S44563 in small-cell lung cancer. *Cell Death Dis*, 5: e1423, September, 2014.

[26] Montero J, Dutta C, van Bodegom D, Weinstock D, Letai A. p53 regulates a non-apoptotic death induced by ROS. *Cell Death Differ*, 20: 1465-1474, November, 2013.

[27] She Q, Bode AM, Ma W. Resveratrol-induced Activation of p53 and Apoptosis Is Mediated by Extracellular- Signal-regulated Protein Kinases and p38 Kinase Resveratrol-induced Activation of p53 and Apoptosis Is Mediated by Extracellular-Signal-Regulated Protein Kinases and p38 Kinase. *Cancer Res*, 61 (4): 1604-1610, February, 2001.

[28] Wu GS. The Functional Interactions Between the p53 and MAPK Signaling Pathways. *Cancer Biol Ther*, 3: 156-161, February, 2004.

[29] Lien J-C, Huang C-C, Lu T-J, Tseng C-H, Sung P-J, Lee H-Z, et al. Naphthoquinone derivative PPE8 induces endoplasmic reticulum stress in p53 null H1299 cells. *Oxid Med Cell Longev*, 2015:453679, 2015.

[30] Chen X, Liao C, Chu Q, Zhou G, Lin X, Li X, et al. Dissecting the molecular mechanism of ionizing radiation-induced tissue damage in the feather follicle. *PLoS One*, 9: e89234, February, 2014.